

Numerical Simulation Analysis of Fluent-based Jet Ladle Baker

Yi Zhao, Lipeng Wang, Changxin Li, Xuebo Chen*

Abstract—To study the influence of the burner on the flame characteristics during the baking process of the jet ladle baker, this paper used the finite element analysis software Fluent to simulate and analyze it. Firstly, the mathematical models of combustion, radiation, and convection heat transfer in the jet ladle roasting process were established by utilizing the energy equation, standard k- ϵ turbulence model, DO radiation model, and component transport model. Then, the effects of several parameters on the flame behavior, including the angle of the obtuse body, the gap between the obtuse body and the gas pipe, the length of the gas pipe that is inserted into the combustion chamber, and the diameter of the combustion chamber, were analyzed through numerical simulations. The results showed that the optimal combustion conditions were achieved when the angle was 60°, the clearance was 20 mm, the length of insertion into the combustion chamber was 50 mm, and the diameter of the combustion chamber was 300 mm. These findings provide a reference for the design of the jet ladle baker and enable a comparison of its performance with that of the conventional baker. The combustion of the jet baker produced a flame with a 61% lower temperature difference and a more stable flame than that of the conventional baker.

Index Term—jet ladle baker, burner, temperature field, numerical simulation

I. INTRODUCTION

As an important piece of equipment connecting the converter, refining furnace, and continuous casting system, the temperature of the ladle significantly impacts the molten steel temperature in the converter and the refining furnace. Ladle baking, as one of the critical processes in steel production, aims to increase the temperature of the ladle lining and remove moisture [1],[2]. Preheating the ladle lining through baking is crucial for enhancing the ladle's service life and boosting billet quality. Before continuous casting, the primary heat loss of molten steel arises from the substantial heat energy absorbed by the ladle [3],[4]. As the ladle baking temperature increases, it becomes feasible to

lower the output temperature of the converter or the refining furnace.

The ladle baking process results from the combination of fluid flow, combustion, and thermal radiation processes [5]. Measuring the internal temperature of the ladle during the baking process is essential for establishing the temperature distribution within the ladle. The previous contact temperature measurement method was accurate [6],[7], but it was complicated to operate and prone to damage. As a result, it is difficult to obtain a complete temperature field of the ladle. Due to the limitations of the contact measurement method, infrared thermometers are commonly used to measure the temperature of the ladle lining [8]-[12]. However, this measurement relies on the values obtained from the thermal effects of the flame radiation inside the ladle. Therefore, the measured values are heavily influenced by the surrounding environment [13]. Additionally, thermal imaging cameras are commonly used tools for measuring temperature fields in ladles [14].

The temperature of the inner wall of the ladle is closely related to the quality of the steel produced and the control of the molten steel temperature. Therefore, measuring the temperature of the ladle is essential for visualizing the temperature control. So far, researchers have achieved the measurement of the inner temperature of the ladle using different methods. For instance, Liu et al. [15] developed a method for scanning the temperature distribution inside the ladle using a Monte Carlo model, which provided theoretical guidance for subsequent effective emissivity correction. It is evident that both the temperature and shape of the flame have a significant impact on the ladle's baking temperature. Meanwhile, Zimmer et al. [16] combined theoretical analysis with experimental data to analyze the heat transfer behavior within the ladle during steelmaking. The results of the study showed that the distribution of the ladle temperature was determined by the contact thermal resistance. On this basis, Tripathi et al. [17] utilized the Computational Fluid Dynamics (CFD) method based on a mathematical model to establish a prediction model of steel temperature inside the ladle. The mathematical model was validated by the collected data. The results showed that the increase in the initial temperature of the refractory material could significantly reduce the molten steel temperature.

The measurement results of ladle temperature can be influenced by a variety of factors. Therefore, only after effective measurement of the temperature can numerical simulation of the temperature field of the ladle be better performed. To further investigate the factors affecting ladle temperature, Yuan et al. [18] used Fluent software to simulate burners with different internal structures of the ladle burner. The internal and external flow fields, as well as the premixed

Manuscript received October 24, 2024; revised April 29, 2025.

This work was supported by the National Natural Science Foundation of China, under grant numbers 71571091 and 71771112.

Yi Zhao is a postgraduate student of School of Electronic and Information Engineering, University of Science and Technology Liaoning, Anshan 114051, China. (e-mail: 13156449651@163.com).

Lipeng Wang is a postgraduate student of School of Electronic and Information Engineering, University of Science and Technology Liaoning, Anshan 114051, China. (e-mail: 17662434145@163.com).

Changxin Li is a network engineer of School of Electronic and Information Engineering, University of Science and Technology Liaoning, Anshan 114051, China. (e-mail: 1367229898@qq.com).

Xuebo Chen is a professor of School of Electronic and Information Engineering, University of Science and Technology Liaoning, Anshan 114051, China. (corresponding author to provide phone: +86 136-1412-8208 ;e-mail: xuebochen@126.com).

combustion reaction of a burner with multiple air holes, were simulated to analyze the flame combustion state within the burner. Huining et al. [19] utilized the finite volume method (FVM) to develop a 3D model that includes in-line preheated combustion and fluid-solid heat transfer, as well as fluid-solid heat transfer for the capping of the ladle and the heavy ladle. They used Fluent software and the weighted sum of gray gas model (WSGGM) to investigate the effect of ladle capping and online preheated ladle lining temperature for regenerative combustion. The results showed that empty ladle capping reduces the molten steel temperature compared to the heavy ladle process. Qi et al. [20] developed a three-dimensional mathematical model to analyze the details of turbulent combustion and the coupled effects of heat transfer phenomena in the ladle baking process. They investigated the efficiencies of oxygen-enriched combustion and air combustion using an improved gray gas weighted sum model. The results showed that oxygen-enriched combustion can save 41.6% of fuel. Umyshev et al. [21] investigated the effect of the obturator distance in the combustion chamber on NO_x emissions. Studies indicated that higher flame temperatures could be obtained with oxygen-enriched combustion, and the increase in flame temperature contributed to the problem of high NO_x emissions. Sun et al. [22] designed a new lightweight ladle with thermal insulation and extended service life to meet the requirements for ladle insulation and durability. Using two methods, a steady-state analysis and a numerical simulation, we analyzed the temperature comparison between the new lightweight ladle and the traditional ladle under the same working conditions. The results proved that the new lightweight ladle has better heat preservation and more uniform temperature field distribution, which is conducive to increasing the service life of the ladle. Zhang et al. [23] conducted a study on the design of a gas injection dual preheating ladle baker. They combined three methods, namely finite element analysis, theoretical analysis, and the basis of engineering practice, to design a new type of gas jet dual preheating ladle baker. The results showed that the gas jet velocity is proportional to the pressure, and it optimized the baker.

By analyzing the baking process of the ladle, we found that the temperature of the ladle can be increased by using different methods to establish the internal temperature field of the ladle for visualization. This increase in the temperature of the ladle significantly affects the temperature of the molten steel. In this paper, the simplified jet ladle baker model was analyzed for combustion simulation using finite element analysis software ANSYS 2023R1. The combustion state of the jet baker was numerically simulated using the energy equation, standard $k-\epsilon$ turbulence model, DO radiation model, and component transfer model. The flame phenomena during combustion for different burner types are investigated, including the angle of the obtuse body (α), the spacing between the obtuse body and the gas pipe (G), the length of the gas pipe extending deeper into the burner (h), and the diameter of the combustion chamber (R). This study provides useful insights for the parameter design of the jet ladle baker burner in practical applications. By comparing it with the traditional ladle baker, the advantages of the jet ladle baker are further highlighted.

II. PHYSICAL MODEL AND MESHING

A. Construction of the physical model

SpaceClaim in ANSYS 2023R1 finite element analysis software is used to model the jet ladle baker with different burner structures and simulate the flow and temperature fields during the ladle baking process in a transient manner. The working principle of the jet ladle baker is as follows: when the ladle is baking, high-pressure gas is ejected through the gap between the gas pipe and the obtuse body, mixing with combustion air in the combustion chamber for combustion. After the gas is ejected through the gap, it flows at high speed, creating a coiling effect that draws in combustion air, resulting in a negative pressure state under the obtuse body. Due to the intense reaction in the combustion chamber and its diameter restricting the flame's diffusion to burn in all directions, the flame can only be directed towards the interior of the ladle. The flame is then ejected from the combustion chamber into the ladle, where it exchanges heat, thereby raising the temperature of the ladle lining.

The simplified model of the jet ladle baker is shown in Fig. 1(a). The model is established in a three-dimensional right-angle coordinate system, where the coordinate origin is located in the center of the bottom of the ladle, and the height of the ladle is oriented in the positive direction of the Z-axis. The jet ladle baker is simplified as consisting of three parts: the ladle, the ladle cover, and the burner. In this paper, the size of the ladle is fixed during the analysis, with a focus on analyzing the baking state under different burner models. The size of the ladle is shown in Fig. 1(b). The simplified burner model mainly includes the gas pipe, the obtuse body, and the combustion chamber. The two-dimensional structure of the burner is shown in Fig. 1(c), where the length of the combustion chamber (H) is 800 mm and the diameter of the gas tube (r) is 100 mm.

In the study of the burner, the four parameters are the angle of the obtuse body (α), the gap (G) between the obtuse body and the gas pipe, the length (h) of the gas pipe extending into the combustion chamber, and the diameter (R) of the combustion chamber. When studying these four parameters, only one is varied at a time for comparison, while the geometry of the ladle model is kept constant. The parameters of the burner geometry model are shown in Table 1. The simulation results are used to compare and analyze the combustion state under different models, providing valuable insights for further parameter optimization in practical applications.

B. Meshing

The obtuse body of the burner is conical in the 3D model of the jet ladle baker created using SpaceClaim. Due to the complex structure of the burner, the Meshing component of Workbench is used to perform unstructured meshing of the model. After the overall division of the ladle baker, the mesh consists of 8.78×10^5 elements. Fig. 2(a) shows the overall division of the ladle baker, while Fig. 2(b) presents the mesh division of the obtuse body. The meshing process divides the ladle baker into four parts: the obtuse body, the combustion region, the ladle cover, and the ladle.

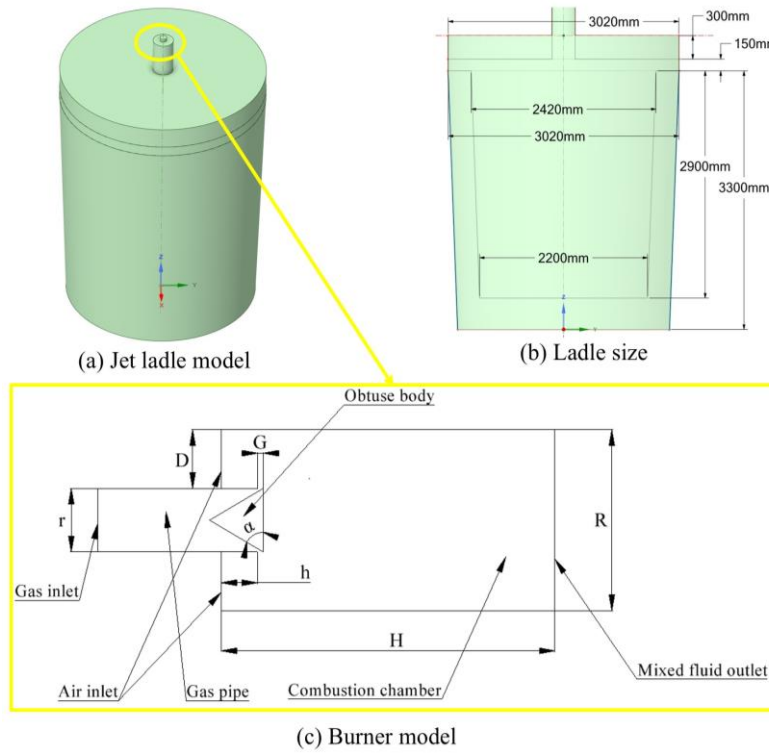


Fig. 1. Jet ladle model and dimensions

TABLE I
PARAMETER TABLE OF BURNER GEOMETRY MODEL

model	obtuse body angle α ($^\circ$)	Gap between obtuse body and gas pipe G (mm)	Length of gas pipe into combustion chamber h (mm)	Combustion chamber diameter R (mm)
1	30	20	50	300
2	45	20	50	300
3	60	20	50	300
4	70	20	50	300
5	60	10	50	300
6	60	20	50	300
7	60	30	50	300
8	60	20	0	300
9	60	20	50	300
10	60	20	100	300
11	60	20	50	200
12	60	20	50	300
13	60	20	50	400

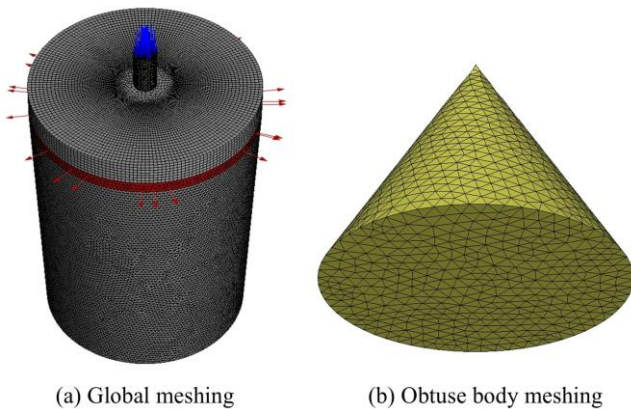


Fig. 2. Mesh delineation diagrams for the ladle as a whole and for the obtuse body

III. NUMERICAL SIMULATION

A. Governing equation

In practical engineering applications, combustion is a

turbulent phenomenon. In the established numerical simulation of ladle baking, the standard k- ϵ model is chosen for the calculations. The turbulence control equations are solved in a closed form, and the viscosity between molecules can be neglected.

The continuity equation [24]:

$$\frac{\partial \rho}{\partial t} + \frac{\partial}{\partial x_j} (\rho \bar{u}_j) = 0 \quad (1)$$

Momentum conservation equation [25]:

$$\begin{aligned} \frac{\partial}{\partial t} (\rho \bar{u}_i) + \frac{\partial}{\partial x_j} (\rho \bar{u}_i \bar{u}_j) = & -\frac{\partial p}{\partial x_j} + \frac{\partial}{\partial x_j} \left[\mu \left(\frac{\partial \bar{u}_j}{\partial x_i} + \frac{\partial \bar{u}_i}{\partial x_j} \right) \right] \\ & - \frac{\partial}{\partial x_j} (\rho \bar{u}_j' \bar{u}_i') - \frac{2}{3} \frac{\partial}{\partial x_j} \left(\mu \frac{\partial \bar{u}_j}{\partial x_j} \right) + \rho g_i \end{aligned} \quad (2)$$

Energy equation:

$$\begin{aligned} \frac{\partial}{\partial t} (\rho \bar{T}) + \frac{\partial}{\partial x_j} (\rho \bar{u}_j \bar{T}) = & \frac{\partial}{\partial x_j} \left(D \rho \frac{\partial \bar{T}}{\partial x_j} \right) \\ & - \frac{\partial}{\partial x_j} (\rho \bar{u}_j \bar{T}') + \bar{Q}_R + \bar{Q}_{rad} \end{aligned} \quad (3)$$

where, ρ is the mainstream density, kg/m³; u is the velocity, m/s; μ is the molecular viscosity coefficient, Pa·s; D is the molecular diffusion coefficient, m²/s; t is the time, s; $i, j=1, 2, 3$; T is the thermodynamic temperature, K; Q_{rad} is the rate of heat transfer from the outside world to the volume, and Q_R is the power of the power of the doing.

Turbulent kinetic energy equation k:

$$\begin{aligned} \frac{\partial}{\partial t} (\rho k) + \frac{\partial}{\partial x_i} (\rho k u_i) = & \frac{\partial}{\partial x_i} \left[\left(\mu + \frac{\mu_t}{\sigma_k} \right) \frac{\partial k}{\partial x_j} \right] \\ & + G_k + G_b - \rho \epsilon - Y_M + S_k \end{aligned} \quad (4)$$

Turbulent kinetic energy dissipation rate equation ϵ :

$$\frac{\partial}{\partial t}(\rho\varepsilon) + \frac{\partial}{\partial x_i}(\rho\varepsilon u_i) = \frac{\partial}{\partial x_j} \left[\left(\mu + \frac{\mu_t}{\sigma_\varepsilon} \right) \frac{\partial \varepsilon}{\partial x_j} \right] + C_{1\varepsilon} \frac{\varepsilon}{k} (G_k + C_{3\varepsilon} G_b) - C_{2\varepsilon} \rho \frac{\varepsilon^2}{k} + S_\varepsilon \quad (5)$$

where, μ_t is the turbulent viscosity coefficient, kg/(m·s); u is the velocity, m/s; G_k represents the turbulent kinetic energy generated by the laminar velocity gradient (shear generation term); G_b is the turbulent kinetic energy generated by buoyancy (volumetric force generation term); Y_M is the fluctuation generated by diffusion in the transition in the compressible turbulence; S_k and S_ε are the customized source phases; σ_k and σ_ε is the turbulence Prandtl number for the k and ε equations, $\sigma_k=1.0$, $\sigma_\varepsilon=1.3$; $C_{1\varepsilon}$, $C_{2\varepsilon}$, $C_{3\varepsilon}$ are empirical constants, $C_{1\varepsilon}=1.44$, $C_{2\varepsilon}=1.92$, $C_{3\varepsilon}=0.09$.

B. Radiation heat transfer model

Radiant heat transfer is one of the main modes of heat transfer in high temperature combustion baking. In the ladle baking process, radiation heat transfer accounts for a large proportion of the total heat transfer. The four radiation models include P1, DO, Rosseland, and DTRM. For ladle baking, the DO discrete-ordinate radiation model solves for the intensity of radiation from a finite number of discrete solid angles. The DO model is widely used and can quickly handle the incident scattering term to simulate the radiation between the gas and the particles. Therefore, the DO radiation model is used to solve the problem in this paper. The number of radiative transport equations corresponds to the number of direction vectors in the spatial coordinate system, as expressed in equation (6). The weighted sum of grey gas model (WSGGM) is also used to calculate the varying absorption coefficients [26],[27].

$$\frac{dI(r,s)}{ds} + (a + \sigma_s)I(r,s) = an^2 \frac{\sigma T^4}{\pi} + \frac{\sigma_s}{4\pi} \int_0^{4\pi} I(r,s')\Phi(s,s')d\Omega' \quad (6)$$

where, r is the position vector; s is the direction vector; s' is the scattering direction; σ_s is the scattering coefficient, 1/s; a is the absorption coefficient, 1/m; n is the refraction coefficient; σ is the Stefan-Boltzmann constant, 5.672×10^{-8} W/(m²·K⁴); I is the total radiant intensity, W/m², depending on the position and direction; T is the local temperature, K; Φ is the scattering phase function of the condensed phase, °; Ω' is the spatial steric angle, rad, indicating the spatial distribution characteristics of inward scattering.

C. Component model

Component transport modeling is performed by solving the conservation equations for convection, diffusion, and reaction of components in a mixture. It also represents the mixing and reaction of chemical substances. Combustion reactions during baking are volumetric reactions related to component transport. The local mass fraction of each substance is predicted by solving the convection-diffusion equation.

$$\frac{\partial \rho c_s}{\partial x} + \text{div}(\rho c_s) = \text{div}[D_s \text{grad}(\rho c_s)] + S_s \quad (7)$$

where, ρ is the density, kg/m³; c_s is the mass fraction of the component, ω ; D_s is the diffusion coefficient of the component s , m²/s; S_s is the source term of the chemical reaction, and the amount of generation per unit time per unit volume through the chemical reaction component s , i.e., the rate of the chemical reaction.

D. Boundary condition setting and model solving

For the combustion reaction, the gas is converter gas and the combustion air is air with 21% oxygen content. The calorific value of the converter gas is 7413 KJ/Nm³. The composition of the converter gas is shown in Table 2. The excess air factor is 1.1. The gas flow rate is 800 m³/h. The gas and air inlets are both velocity inlet boundaries: the gas velocity inlet flow rate is 28.3 m/s with an initial temperature of 300 K; the air velocity inlet flow rate is 5.7 m/s with an initial temperature of 300 K. The outlet boundary is a pressure outlet boundary and the pressure magnitude is atmospheric pressure. Standard wall functions are used for the walls of the ladle. The multi-layer heat-resistant material of the ladle lining was idealized as a single layer, the properties of which are shown in Table 3.

TABLE 2
CONVERTER GAS COMPOSITION TABLE

Component	CO	CO ₂	H ₂	N ₂	O ₂	H ₂ O
Volume concentration %	60.2	14.6	1	18.3	0.2	5.7

TABLE 3
Composition of lining materials

Name	Density factor	Specific heat factor	Thermal conductivity factor
Value	2860kg/m ³	803+0.618×10 ⁻³ J/(kg·K)	5.314-3.37×10 ⁻³ W/(m·K)

When the mathematical simulations were carried out, transient solutions were performed using the pressure basis of Fluent software. The finite volume method and the velocity-pressure coupling algorithm SIMPLEC were used to solve the simulation model.

IV. MODEL VALIDATION

The actual gas used in the plant is coke oven gas, which is combusted with combustion air containing 21 % oxygen. The dimensions of the ladle are 3240 mm in diameter at the bottom, 3840 mm in diameter at the top, and 4060 mm in overall height. The gas flow rate during baking is 430 m³/h. The preheating temperature of the combustion air is 300 K, and the air-fuel ratio is 4:1. Fig. 3 shows the locations of the monitoring points in the actual thermocouple testing. The monitoring points are labeled A, B, C, and D.

The mathematical model developed in this paper is applied to the ladle structure and working conditions in the field for validation. Table 4 presents the on-site and simulated temperatures at the monitoring points.

As shown in Table 4, the temperature within the ladle gradually decreases from the bottom to the top of the ladle.

V. SIMULATION RESULTS AND ANALYSIS

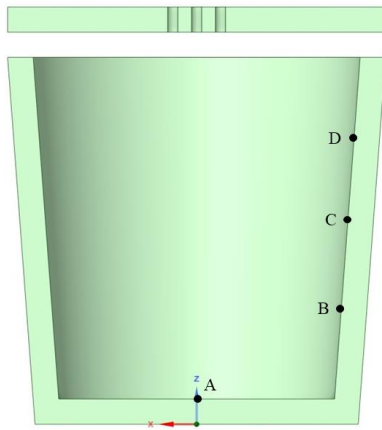


Fig. 3. Thermocouple test point location diagram

TABLE 4
Measured and simulated values

Temperature measurement point	A	B	C	D
Actual measured value /K	1558	1485	1432	1383
Simulated value /K	1480	1436	1431	1414
Relative error /%	-5.01	-3.30	-0.07	2.24

The actual test results under this baking process showed a $\pm 5\%$ error compared to the simulated results. The accurate characterization of the mathematical model can be demonstrated, making it suitable for subsequent calculations in this study. The simulation calculated a 37.7% reduction in flame temperature difference compared to the actual measurement.

A. The effect of obtuse body angle α on combustion state

Models 1-4 in Table 1 are simulated for obtuse body angle α . The obtuse body angles are 30° , 45° , 60° , and 70° . The velocity cloud of different obtuse body angles during combustion baking is shown in Fig. 4, and the temperature cloud is shown in Fig. 5. Gas and air are first mixed and combusted in the combustion chamber to form a high temperature flame which is injected into the ladle. The high temperature flame raises the temperature of the ladle lining through heat radiation and heat exchange. Figure 4 clearly shows that the high temperature flame produced by the combustion of gas and air increases the flow rate inside the ladle as the angle increases. However, as shown in Fig. 5, the temperature field inside the ladle tends to decrease with an increase in the obtuse body angle.

Figure 6 shows the temperature inside the ladle at $Z = 2\text{ m}$ in the X-Z plane, with $Y = 0\text{ m}$. Combining Figures 5 and 6, it is evident that the high temperature flames are located in the center of the ladle. The temperature of the flame gradually decreases towards the bottom of the ladle after being ejected from the combustion chamber. At the same gas flow rate into the gas pipe, increasing the angle of the obtuse body is equivalent to reducing the exit area, resulting in a higher flow rate at the gas pipe exit. In Fig. 6, the highest temperatures at the four angles are 1997 K, 1981 K, 1957 K, and 1939 K, while the lowest temperatures are 1803 K, 1790 K, 1783 K, and 1768 K, respectively. For $\alpha = 30^\circ$ and $\alpha = 45^\circ$, there is a

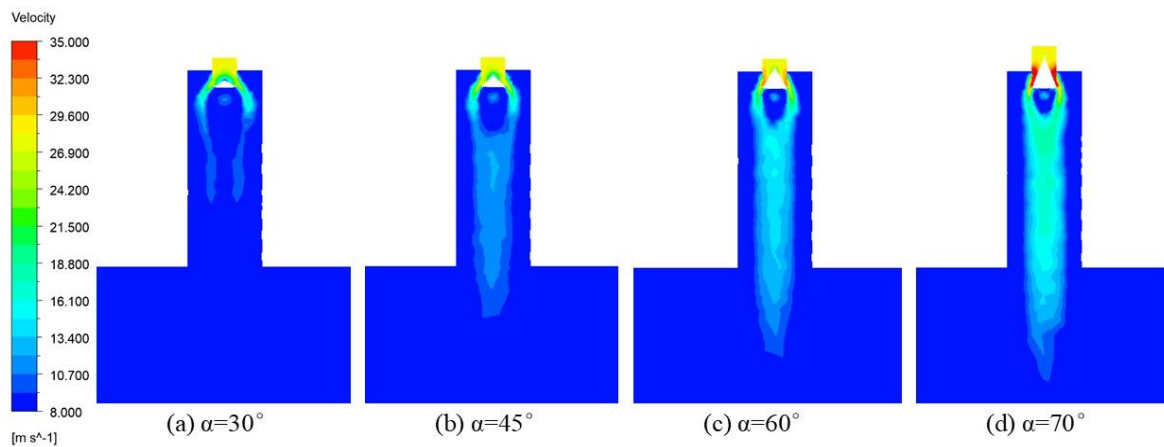


Fig. 4. Velocity clouds at different blunt body angles

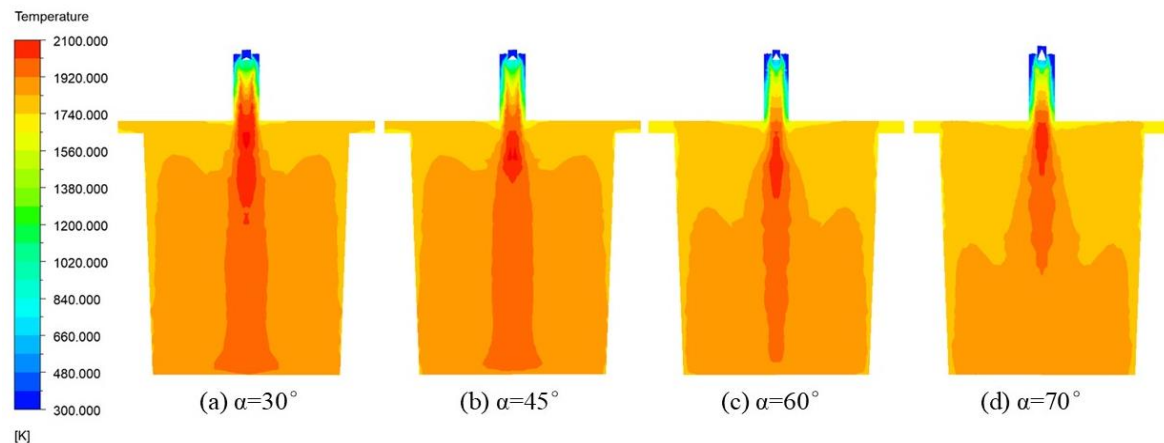


Fig. 5. Temperature clouds at different blunt body angles

temperature difference of 10-15 K only at the center of the flame, with little difference at the other positions. The flame temperature at $\alpha = 60^\circ$ is noticeably higher than at $\alpha = 70^\circ$.

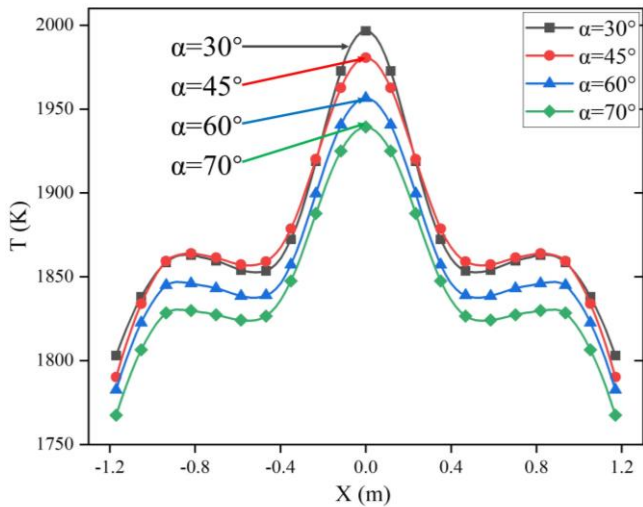


Fig. 6. Temperature distribution for different obtuse body angles α at $Z = 2$ m in the X-Z plane

The temperature from the bottom of the ladle liner ($Z = 0.4$ m) to the bottom of the obtuse body of the burner is shown in Fig. 7, which represents the temperature profile along the positive direction of the Z-axis from the origin. The flame generated by the combustion primarily bakes and heats the ladle liner from the bottom of the ladle liner to a height of $Z = 3.3$ m. The temperature difference in this region needs to be minimized to prevent excessive temperature variation within the ladle. As shown in Fig. 7, the temperature difference at $\alpha = 60^\circ$ is the smallest, at 130 K. The other three angles exhibit a temperature difference of more than 130 K in the vertical direction. Since the high temperature resistance of refractory materials is determined by their inherent material properties, the heating rate of the ladle lining during the heating process should not exceed the tolerance limit of these materials. Excessive temperatures may damage the high temperature resistant materials inside the ladle, potentially causing the lining to blow out or detach, leading to irreversible damage. The four cases are analyzed and compared in combination with Figures 4 to 7. The burning state of the flame at $\alpha = 60^\circ$ is the most consistent with the actual conditions in the project.

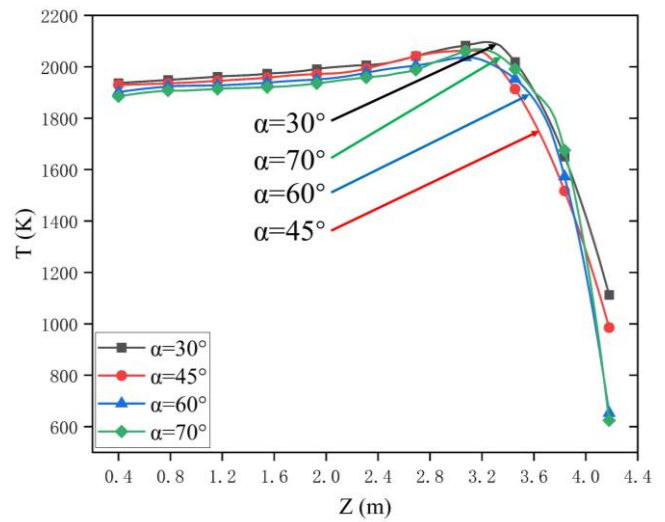


Fig. 7. Temperature map along the positive direction of the Z-axis at the origin at different obtuse body angles α

B. Influence of the gap G between the obtuse body and the gas pipe on the state of combustion

The three models, models 5-7 in Table 1, are simulated to investigate the effect of the size of the gap G between the obtuse body and the gas pipe on the combustion condition. Due to the difference in the gap between the obtuse body and the gas pipe, the reaction rate of the gas and air will vary, resulting in different effects during combustion. The velocity cloud during ladle baking under these three models is shown in Fig. 8, and the temperature cloud is shown in Fig. 9. As shown in the velocity cloud in Fig. 8, the gas flow rate decreases as the gap increases. However, as shown in the temperature cloud in Fig. 9(a), the high temperature flame region is less effective than in the other two cases. This is because the pressure at the gas outlet decreases after the same flow rate of gas is ejected from the gas pipe with a larger relative area. The rapid reaction between the gas and air in the combustion chamber produces a flame that is ejected from the combustion chamber into the inner ladle, creating a turbulent flow of gas inside the ladle. The high temperature flue gas generates eddy currents inside the ladle and radiates to the ladle lining, raising the temperature of the lining.

Figure 10 shows a plot of the temperature data along the positive direction of the Z-axis at the origin, indicating that the flame temperatures in the combustion region from $Z = 0.4$

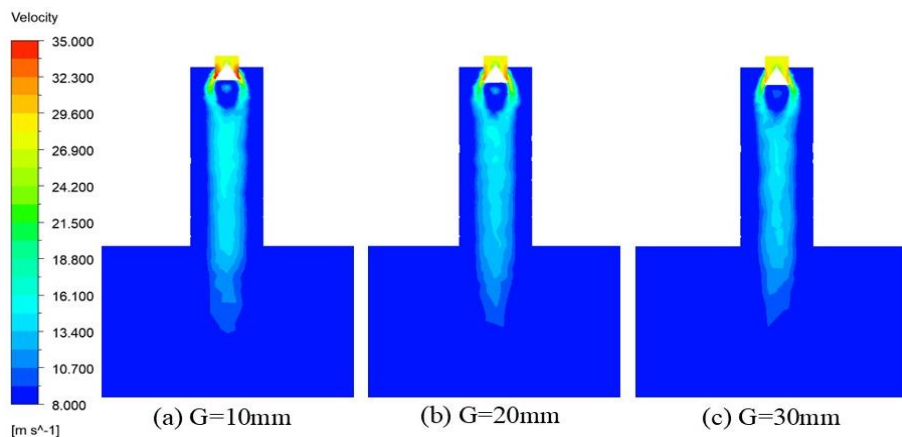


Fig. 8. Velocity clouds for different gap sizes G between the obtuse body and the gas pip

m to $Z = 2.4$ m do not produce a significant difference. However, a more noticeable temperature difference is observed in the combustion region from $Z = 2.4$ m to $Z = 3.3$ m. In these three cases, the flame temperature differences resulting from the combustion reaction between $Z = 0.4$ m and $Z = 3.3$ m are 140 K, 130 K, and 136 K. The flame temperature difference is smallest at $G = 20$ mm, leading to a more uniform flame temperature inside the ladle. It can also be seen from Fig. 11 that the temperature near the inner wall of the ladle is lower at $G = 10$ mm compared to the other two

cases. Although the temperature at $G = 30$ mm in Fig. 11 is higher than that at $G = 20$ mm at the center position, the temperature difference at other positions is relatively small and negligible compared to the overall ladle temperature. Combining Figs. 8 to 11, the baking temperature with $G = 20$ mm results in a more uniform temperature field inside the ladle. Therefore, the working condition with a gap of $G = 20$ mm between the obtuse body and the gas pipe is more suitable for practical application.

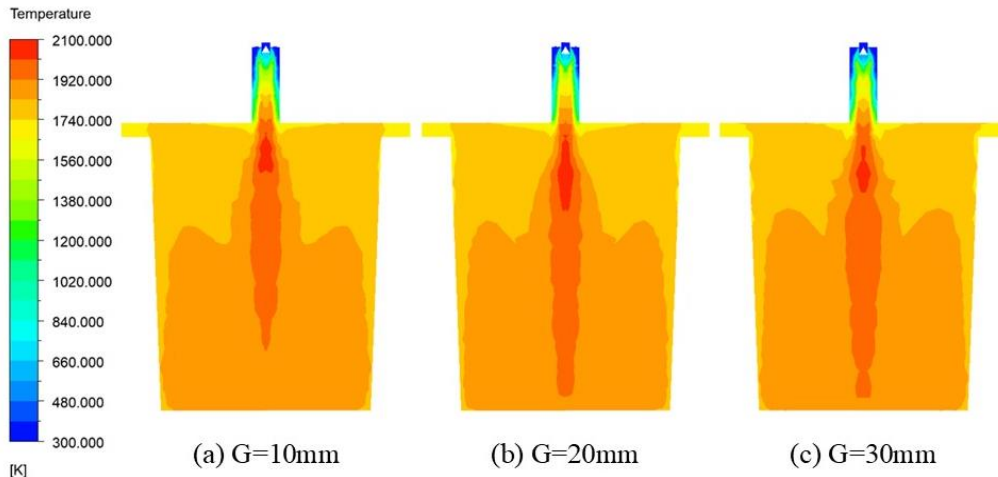


Fig. 9. Temperature clouds with different gap sizes G between the obtuse body and the gas pipe

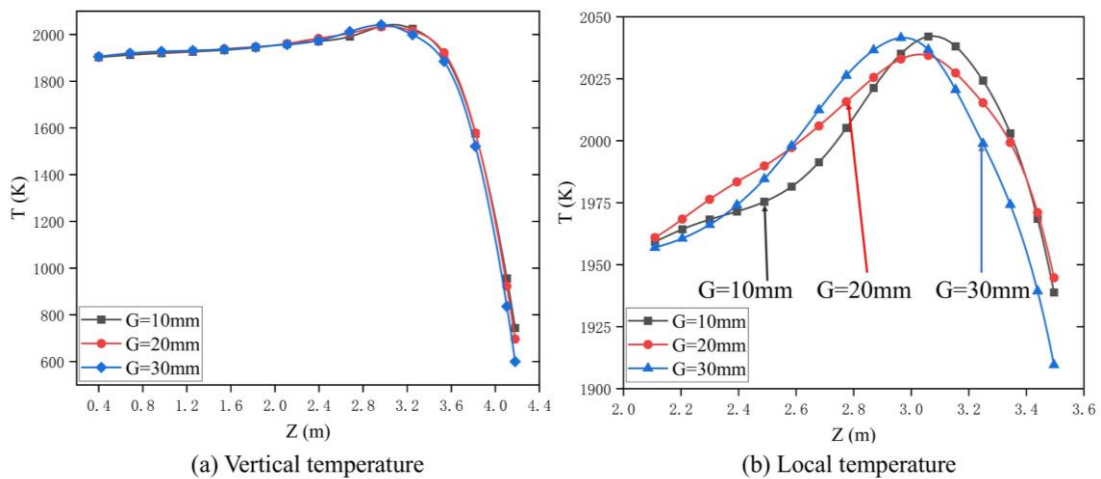


Fig. 10. Temperature along the positive direction of the Z -axis at the origin when the gap G between the obtuse body and the gas pipe is different

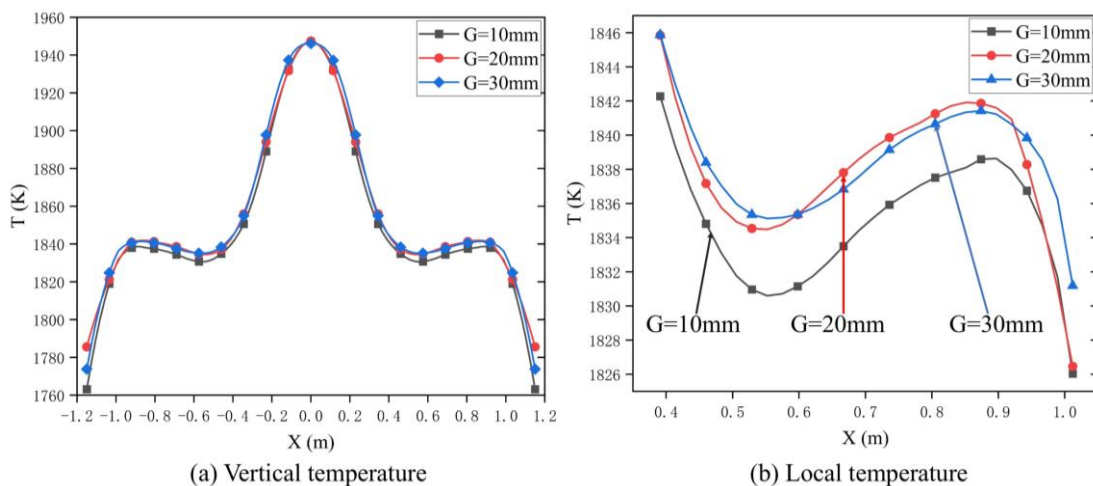


Fig. 11. Temperature distribution of gap G between different obtuse body and gas pipe at X - Z plane $Z = 2$ m

C. Effect of the length h of the gas pipe deep into the combustion chamber on the state of combustion

The position of the gas pipe outlet impacts the combustion reaction, thereby determining the starting position of the flame in the combustion chamber. Models 8-10 in Table 1 were simulated to analyze the effect of the length h of the gas pipe extending into the combustion chamber on the combustion state. In the combustion simulation, the velocity cloud is shown in Fig. 12, and the temperature cloud is shown in Fig. 13.

As shown in Fig. 12, as the length of the gas pipe extending deeper into the combustion chamber increases, the gas flow rate after combustion gradually decreases. This is due to the fact that the contact between the gas and air is reduced when the gas is ejected from the gas pipe, causing the reaction to slow down. From Fig. 13, it can be seen that as the gas pipe extends deeper, the high temperature region of the flame moves progressively closer to the ladle. The temperature cloud in Fig. 13(a) clearly shows a significant difference in the combustion chamber compared to the other two cases.

Figure 14 presents the temperature distribution along the Z-axis at the origin, directly reflecting the temperature profile of the flame at the ladle's center. When the gas pipe is deeply inserted into the combustion chamber with a length of $h = 0$ mm, the end of the gas pipe is at the same height as the top of the combustion chamber, allowing the gas to quickly coil and draw in combustion air to react, forming a high temperature flame. In Fig. 14, the temperature at the top for $h = 0$ mm is higher than in the other two cases, with a maximum

temperature of 2186 K. From Fig. 13(b) and (c), it can be clearly observed that the high temperature flame generated by the reaction between the cold combustion air and the gas at $h = 100$ mm is shorter than that at $h = 50$ mm. This causes the small temperature variation from $Z = 2.8$ m to $Z = 3.2$ m in Fig. 14.

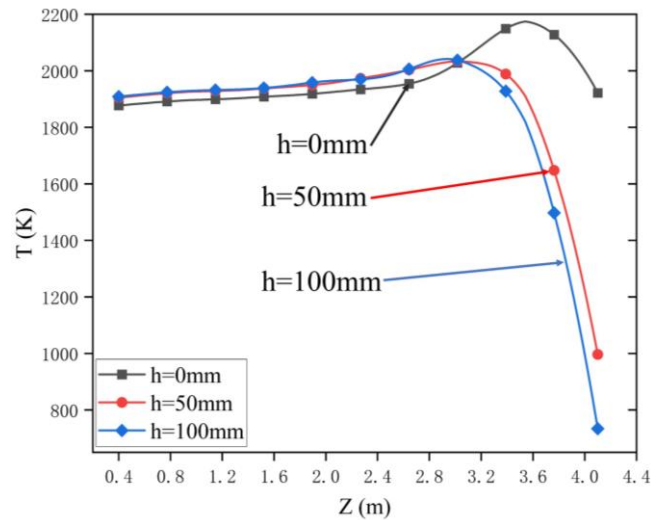


Fig. 14. Temperature in the positive direction of the Z-axis at the origin for different lengths h of the gas pipe deep into the combustion chamber

Figure 15 shows the temperature inside the ladle at the X-Z plane $Z=2$ m at $Y=0$ m. The longer the length of the gas pipe extending deeper into the combustion chamber, the higher the

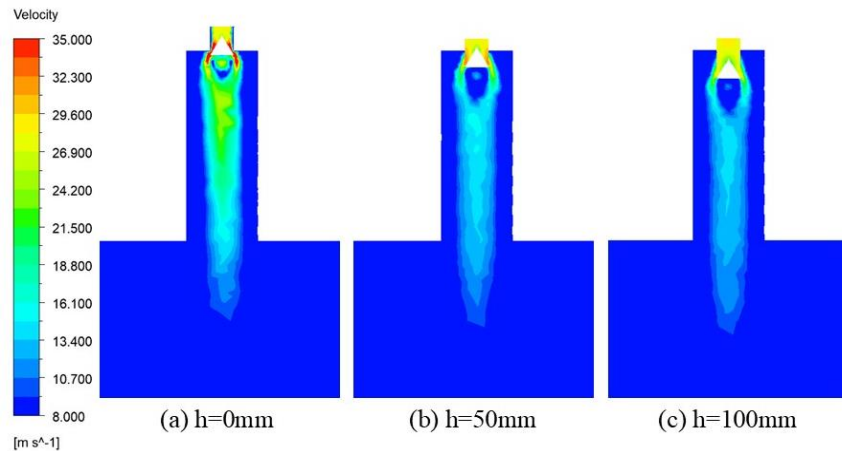


Fig. 12. Velocity clouds when the gas pipe penetrates deeper into the combustion chamber with different lengths

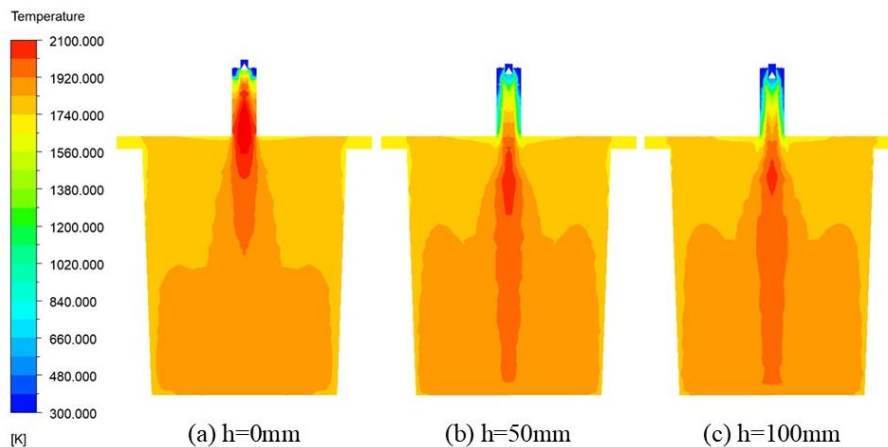


Fig. 13. Temperature clouds at different lengths h of the gas pipe into the combustion chamber

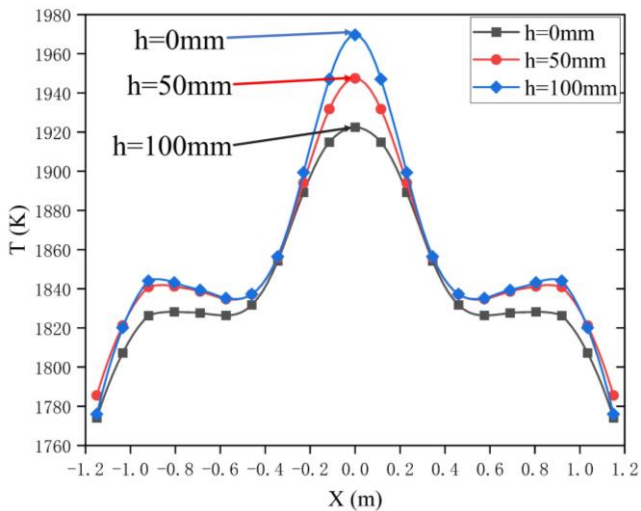


Fig. 15. Temperature in the X-Z plane Z = 2 m ladle at different times when the gas pipe penetrates deep into the combustion chamber length h

temperature at the center. When $h = 0$ mm, the temperature is significantly lower than in the other two cases. Although the highest temperature at the center is 1970 K for $h = 100$ mm, the temperature near the inner wall of the ladle is noticeably lower than at $h = 50$ mm. The average temperature of the baking area shown in Fig. 15 is 1815 K, 1827 K, and 1824 K for cases (a), (b), and (c), respectively, with the highest average temperature occurring at $h = 50$ mm. After comprehensive analysis, when the baking time is the same, the flame generated at $h = 50$ mm makes the temperature

uniformity inside the ladle better. The ladle lining will not cause excessive temperature differences and reduces the absorption of molten steel heat by the ladle lining. Based on the above analysis, $h = 50$ mm is more suitable for practical ladle baking applications.

D. Effect of combustion chamber diameter R on combustion state

The diameter of the combustion chamber directly affects the amount of combustion air intake, and different baking results are formed due to changes in the contact area between the gas and air. Models 11-13 in Table 1 were simulated to analyze the combustion response for different combustion chamber diameters. The simulated velocity cloud for the baking process when only the combustion chamber diameter is changed is shown in Fig. 16, and the temperature cloud is shown in Fig. 17. The temperature inside the ladle is also related to the degree of air-gas mixing during combustion; the better the mixing, the higher the flame temperature. As shown in the velocity cloud in Fig. 16(a), it is found that a large amount of gas is sprayed onto the inner wall of the combustion chamber, which cannot mix with the combustion air sufficiently for combustion. Complete combustion of the gas requires sufficient oxygen; however, the diameter of the combustion chamber limits the entry of combustion air.

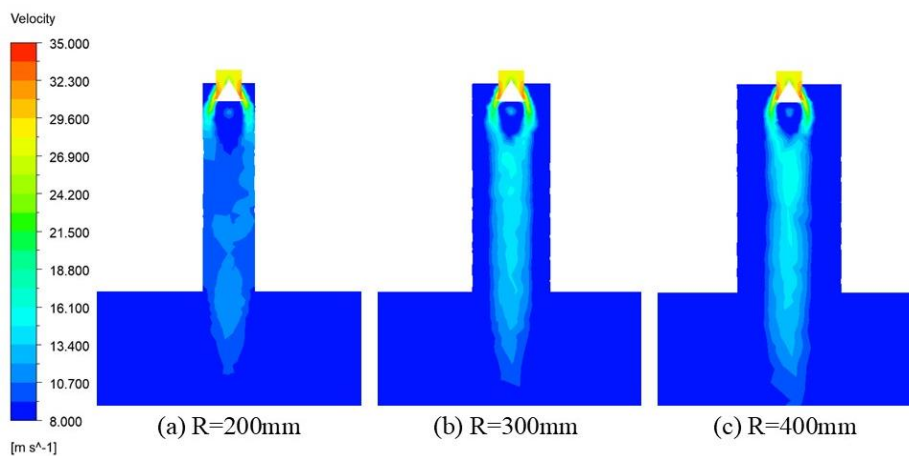


Fig. 16. Velocity clouds for different combustion chamber diameters R

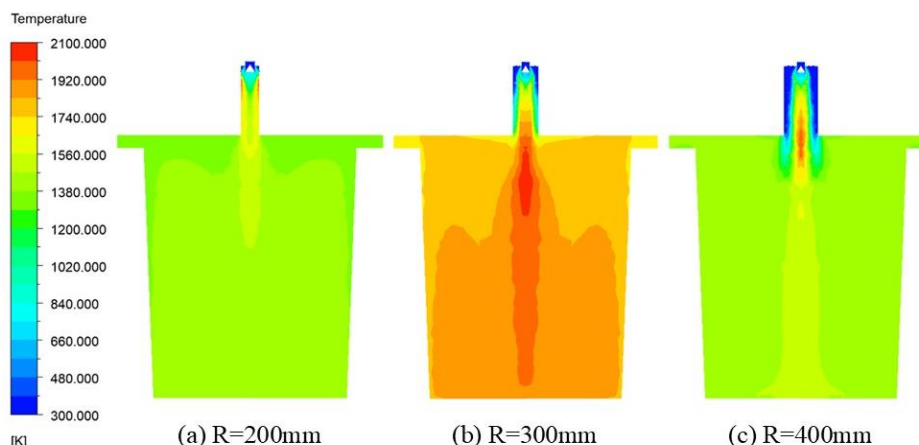


Fig. 17. Temperature clouds for different combustion chamber diameters R

It can also be observed from Fig. 17(a) that the gas does not produce a higher ambient temperature after combustion. Therefore, the combustion reaction at $R = 200$ mm is insufficient, and the combustion rate will not increase, nor will there be a strong impact when the flame is ejected from the combustion chamber. As shown in Fig. 17, the temperature in the ladle is highest only when the diameter of the combustion chamber $R = 300$ mm. The average temperature inside the ladle in these three cases is 1025 K, 1030 K, and 1026 K, respectively, with maximum temperatures of 1163 K, 1361 K, and 1170 K. This shows that it is not the case that the larger the diameter of the combustion chamber, the better. When it is larger, a large amount of cold air is drawn in during the combustion process between the gas and the combustion air. The room temperature air needs to absorb a lot of heat within the high temperature field of the ladle, resulting in lower temperatures on both sides of the high temperature flame.

Figure 18 presents the temperature distribution inside the ladle along the positive direction of the Z-axis from the origin. As shown in the figure, the temperature at $R = 200$ mm is significantly lower than in the other two cases, with a maximum temperature of 1568 K. When the diameter of the combustion chamber is too large at $R = 400$ mm, although the gas and combustion air mix completely during combustion, the excessive intake of air prevents an intense combustion reaction. Figure 18 shows that the high temperature area at $R = 400$ mm is mainly located in the upper part of the combustion chamber and ladle, resulting in a significant temperature difference of 500 K. Combining the analysis and comparison of the three states in Fig. 16 to Fig. 18, the temperature inside the ladle is highest and the temperature difference is smallest (135 K) when $R = 300$ mm. With the same time and gas flow rate, the temperature inside the ladle increases the most when $R = 300$ mm. Therefore, the structure with $R = 300$ mm should be selected as the diameter of the combustion chamber.

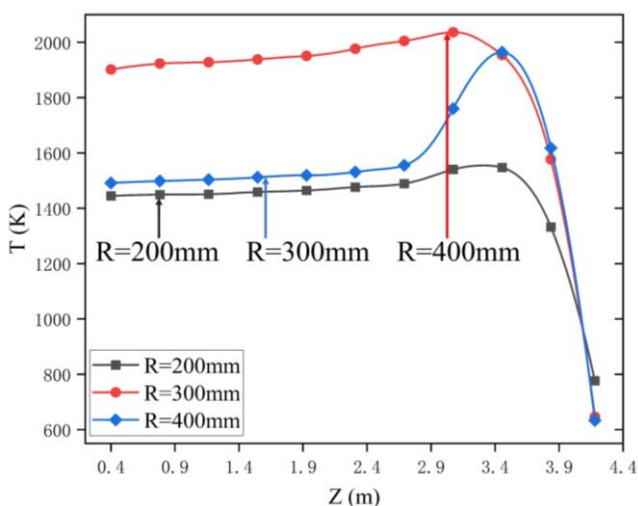


Fig. 18. Temperature distribution along the Z-axis at the origin for different combustion chamber diameters R

VI. COMPARISON OF JET BURNER AND TRADITIONAL BURNER

The biggest difference between traditional and jet burners lies in the burner structure. The traditional burner inserts the

gas and air pipes directly into the steel ladle for baking. The half-sectional view of the conventional burner model in the X-Z plane at $Y = 0$ m is shown in Fig. 19(a), with a magnified view of the burner part in Fig. 19(b). The diameter of the gas pipe is 100 mm, and the diameter of the air pipe is 300 mm. After determining the burner model, the jet steel ladle burner is shown in Fig. 20, where (a) is the sectional view of the X-Z plane at $Y = 0$ m, and (b) shows the burner part of the jet burner. Fluent was used to simulate the baking process for thirty minutes with both types of burners. The same mathematical model was applied in both simulations, using converter gas with a flow rate of $600\text{m}^3/\text{h}$ and an air-fuel ratio of 4:1, with an excess air ratio of 1.1:1. The oxidizing gas used was air with 21% oxygen content.

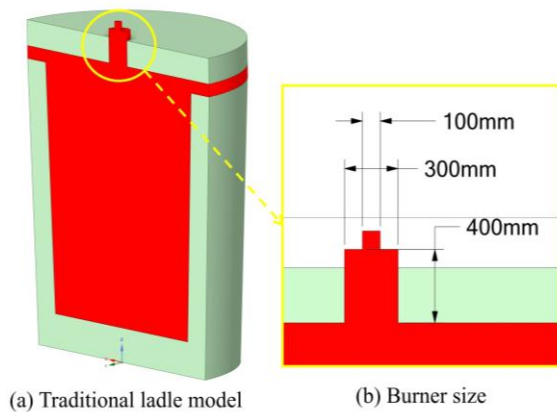


Fig. 19. Simplified diagram of traditional ladle baker

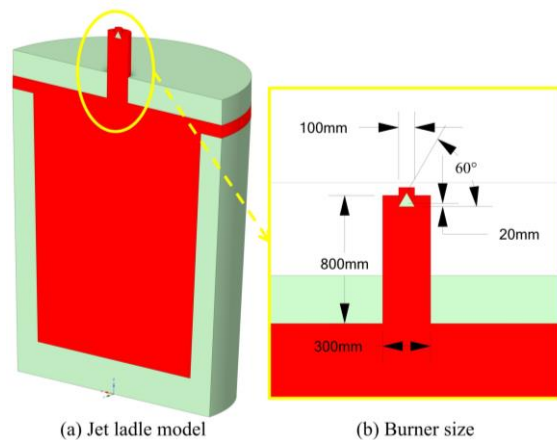


Figure 20. Simplified diagram of jet ladle baker

Temperature clouds during roasting are illustrated in Fig. 21, where (a) represents a conventional baker and (b) represents a jet baker. The jet baker clearly produces higher temperatures than the conventional baker when the gas is burned. The length of the high temperature flame in the jet baker is longer than that in the conventional baker. Owing to the temperature difference of the flame in the vertical direction during the roasting process, the internal ambient temperature of the ladle varies accordingly. The maximum temperature of the baking environment of the traditional baker is 2179 K, with an average temperature of 1775 K. In contrast, the jet baker's baking environment reaches a maximum temperature of 2205 K and has an average temperature of 1858 K. The difference in maximum temperature between these two cases is 26 K, and the

difference in average temperature is 83 K.

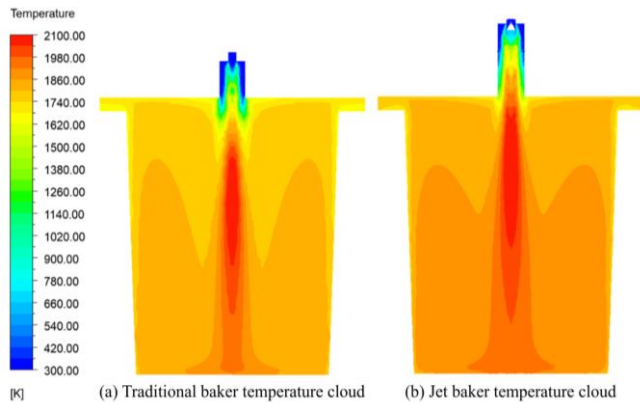


Fig. 21 Temperature cloud of the two bakers at the time of baking

The analysis of the flame along the center of the vertical direction from 0.4m to 3.4m is shown in Figure 22. The flame temperature difference produced by the jet baker after combustion is significantly smaller than that of the traditional baker. The maximum temperature of the traditional baker reaches 2139 K, while the maximum temperature of the jet baker reaches 2176 K, showing a difference of 37 K. The minimum temperature of the conventional baker is 1537 K, which is a difference of 602 K from the maximum temperature.

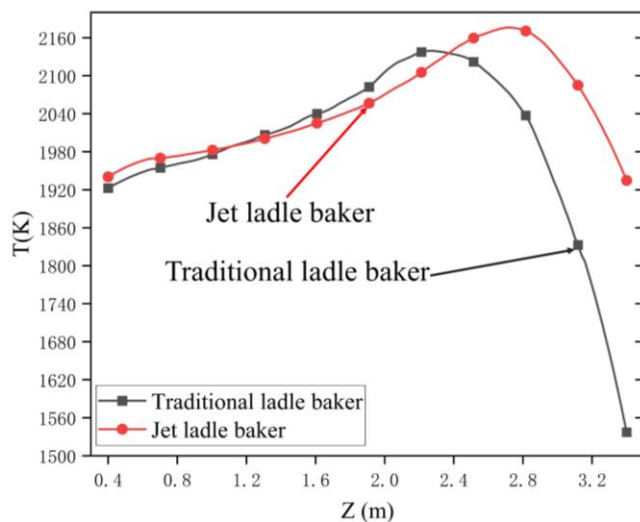


Fig. 22. Flame temperature analysis in vertical direction

This indicates that the flame temperature uniformity is poorer, which may lead to a larger temperature difference in the ladle lining. The minimum temperature of the jet baker is 1940 K, and the temperature difference from the maximum temperature is 236 K, which is about 61 % lower than the temperature difference of the conventional baker. The ambient temperature inside the ladle during the baking process clearly shows that the baking temperature of the jet baker is superior.

After the above analysis of the temperature produced by the mixture of gas and combustion air from the two types of bakers, it can be concluded that the flame uniformity and the temperature difference produced by the jet baker are more advantageous than those of the conventional baker. Therefore, the jet baker has a better baking effect.

VII. CONCLUSION

This paper demonstrates the effect of the burner portion of the jet ladle roaster on the flame during combustion. Numerical simulations were conducted to simulate the combustion conditions of jet ladle bakers under different burner configurations. The conclusions are as follows:

1) As the angle of the obtuse body increases, the temperature along the direction of the flame decreases, and the temperature field inside the ladle gradually becomes lower. It is important to note that while jet baking directs the flame to the bottom of the ladle, excessively high temperatures can overbake the center of the ladle, leading to uneven temperature distribution. Considering all these factors, it is clear that an obtuse body angle of 60° should be chosen.

2) As the gap between the obtuse body and the gas pipe widens, the temperature field inside the ladle first increases and then decreases. When the gap is too small, the amount of gas ejected is insufficient, and the flame that burns after reacting with the combustion air lacks sufficient rigidity. When the gap is too large, too much gas is sprayed in, resulting in a waste of resources. The analysis clearly shows that a gap of 20 mm between the obtuse body and the gas pipe is the most suitable option.

3) As the length of the gas pipe deep into the combustion chamber increases, the high temperature zone of the flame during combustion gradually shifts downward, and the rigidity of the flame increases. The purpose of roasting is to raise the temperature of the ladle lining, which must be achieved by directing the high temperature area of the flame towards the ladle. A gas pipe length of 50 mm deep into the combustion chamber is the most practical option.

4) The diameter of the combustion chamber directly affects the entry of combustion air. The temperature field inside the ladle does not increase with the increasing diameter of the combustion chamber. When too little combustion air enters, the gas reaction is incomplete; when too much combustion air enters, it flows with the flame into the ladle, bringing lower-temperature air. A combustion chamber diameter of 300 mm is the optimal choice to achieve the best combustion results.

5) Jet bakers provide a higher degree of fuel combustion efficiency than traditional bakers, increasing the average temperature of the baking in the ladle and reducing the temperature gap of the flame by 61 %, which results in an increase in the flame's rigidity.

REFERENCES

- [1] H. Tsuji, A.K. Gupta, T. Hasegawa, M. Katsuki, K. Kishimoto, and M. Morita, *High Temperature Air Combustion: From Energy Conservation to Pollution Reduction*. CRC Press, 2002.
- [2] F. Yuan, H Wang, P Zhou, A Xu, and D He, "Heat transfer performances of honeycomb regenerators with square or hexagon cell opening," *Applied Thermal Engineering*, vol. 125, pp. 790-798, Oct. 2017.
- [3] S. Thompson, and M. Si, "Strategic analysis of energy efficiency projects: Case study of a steel mill in Manitoba," *Renewable and Sustainable Energy Reviews*, vol. 40, pp. 814-819, Dec. 2014.
- [4] B.S. Chaikin, G.E. Mar'yanchik, E.M. Panov, P.T. Shaposhnikov, V.A. Vladimirov, I.S. Volovik, and B.A. Makarevich, "State-of-the-art plants for drying and high-temperature heating of ladles," *Refractories and Industrial Ceramics*, vol. 47, pp. 283-287, Sep. 2006.

- [5] J. Rieger, M. Drózd-Ryś, C. Weiss, and H. Harmuth, "Thermochemical Wear of Refractory Linings Associated With Gas Firing in Metallurgical Plants," *Steel Research International*, vol. 85, no. 4, pp. 527-536, Apr. 2014.
- [6] L.E. Jardón-Pérez, A.M. Amaro-Villeda, G. Trápaga-Martínez, C. González-Rivera, and M.A. Ramírez-Argáez. "Utilization of the Planar Laser-Induced Fluorescence Technique (PLIF) to Measure Temperature Fields in a Gas-Stirred Ladle," *Metallurgical and Materials Transactions B*, vol. 51, pp. 2510-2521, Aug. 2020.
- [7] G. Phanomchoeng, S. Chantranuwathana, and P. Charunyakorn, "On-line Ladle Lining Temperature Estimation by Using Bounded Jacobian Nonlinear Observer," *Journal of Iron and Steel Research International*, vol. 23, pp. 792-799, Aug. 2016.
- [8] H.O. Garces, L. Arias, A.J. Rojas, C. Carrasco, A. Fuentes, and O. Farias, "Radiation measurement based on spectral emissions in industrial flames," *Measurement*, vol. 87, pp. 62-73, June 2016.
- [9] B. Glaser, M. Görnerup, and D. Sichen, "Thermal Modelling of the Ladle Preheating Process," *steel research international*, vol. 82, no. 12, pp. 1425-1434, Dec. 2011.
- [10] I. Jain, R.-K. Singh, and D. Mazumdar, "Measurements of Some Thermal Properties of Steel-Refractory Systems and Heat Losses from Steelmaking Furnaces," *Transactions of Indian Institute of Metals*, vol. 68, pp. 383-392, Nov. 2014.
- [11] D. Gruber, and H. Harmuth, "Thermomechanical Behavior of Steel Ladle Linings and the Influence of Insulations," *steel research international*, vol. 85, no. 4, pp. 512-518, Apr. 2014.
- [12] V.A. Kononov, and I.I. Zemskov, "Modern high-temperature thermal insulation for steel-pouring ladles," *Refractories and Industrial Ceramics*, vol. 53, no. 3, pp. 151-156, Nov. 2012.
- [13] R.I. Iacobescu, G.N. Angelopoulos, P.T. Jones, B. Blanpain, and Y. Pontikes, "Ladle metallurgy stainless steel slag as a raw material in Ordinary Portland Cement production: A possibility for industrial symbiosis," *Journal of Cleaner Production*, vol. 112, pp. 872-881, Jan. 2016.
- [14] M. Doubenskaia, M. Pavlov, S. Grigoriev, and I. Smurov, "Definition of brightness temperature and restoration of true temperature in laser cladding using infrared camera," *Surface and Coatings Technology*, vol. 220, pp. 244-247, April 2013.
- [15] J. Liu, Y.H. Huang, Y. Ci, J.X. Fang, F. Yang and N. David, "Inner wall temperature distribution measurement of the ladle based on cavity effective emissivity correction," *Scientific Reports.*, vol 12, Jan. 2022.
- [16] A. Zimmer, Á.N.C. Lima, R.M. Trommer, S.R. Bragança, and C.P. Bergmann, "Heat Transfer in Steelmaking Ladle," *Journal of Iron Steel Research International* vol. 15, pp. 11-14, March 2008.
- [17] A. Tripathi, J. K. Saha, J. B. Singh, and S. K. Ajmani, "Numerical Simulation of Heat Transfer Phenomenon in Steel Making Ladle," *ISIJ International*, vol. 52, pp. 1591-1600, 2012.
- [18] F. Yuan, H.B. Wang, P.L. Zhou, and A.J. Xu, "Combustion performance of nozzles with multiple gas orifices in large ladles for temperature uniformity," *Journal of Iron Steel Research International*, vol. 25, pp. 387-397, April 2018.
- [19] H. Zhang, P. Zhou, and F. Yuan, "Effects of ladle lid or online preheating on heat preservation of ladle linings and temperature drop of molten steel," *Energy*, vol 214, 2021.
- [20] F. Qi, J. Shan, B. Li, and J. Baleta, "Numerical Study On Ladle Baking Process Of Oxy-Fuel Combustion," *Thermal Science*, vol. 24, pp. 3511-3520, 2020.
- [21] D.R. Umyshev, A.M. Dostiyarov, A.A. Kibarin, G.M. Tyutebayeva, G.S. Katranova, and D.B. Akpanbetov, "Experimental investigation of distance between v-gutters on flame stabilization and NOx emissions," *Thermal Science*, vol. 23, pp. 2971-2981, 2019.
- [22] Y. Sun, J. Tian, J. Du, B. Tao, Y. Liu, J. Yun, D. Chen, "Numerical simulation of thermal insulation and longevity performance in new lightweight ladle," *Concurrency and Computation: Practice and Experience*, vol. 32, June 2020.
- [23] Z X Zhang, L Fu and M B Zheng, "Design and Application on the Gas Jet Double Preheated Ladle Baker," *IOP Conference Series: Earth and Environmental Science*, vol. 186, 2018.
- [24] T. Cheng, R. Zhu, and K. Dong, "Effect of methane-hydrogen mixtures on flow and combustion of coherent jets," *Journal of Iron and Steel Research International*, vol. 24, pp. 1143-1151, Nov. 2017.
- [25] Y.B. He, W.K. Guo, Y.H. Li, G.M. Liu, and X. Cui, "Numerical simulation of flow characteristics of side-bottom combined blowing in iron bath reactor," *Journal of Iron and Steel Research International*, vol. 30, pp. 236-248, Feb. 2023.
- [26] W.A. Fiveland, "Discrete-Ordinates Solutions of the Radiative Transport Equation for Rectangular Enclosures," *ASME. Journal of Heat and Transfer*, vol. 106, pp. 699-706, Nov. 1984.
- [27] J.S. Truelove, "Discrete-Ordinate Solutions of the Radiation Transport Equation," *ASME. Journal of Heat and Transfer*, vol. 109, pp. 1048-1051, Nov. 1987.